Journal of Sound and Vibration (1997) **205**(5), 712–720

THE IMPACT OF FLEXIBLE LINKS WITH SOLID LUBRICATION

D. B. MARGHITU
Department of Mechanical Engineering, Auburn University, Auburn, AL 36849, *U.S.A.*

(*Received* 20 *November* 1996, *and in final form* 12 *March* 1997)

1. INTRODUCTION

Switches, connectors and electrical contacts are ubiquitous elements in today's "more electric society". Despite various design directions which might be thought to reduce the number of make-break electromechanical contacts, contacts still provide the largest single source of failure in automotives, aircraft, machine tools, computers, and consumer electronics. While great advances in quality, performance, packaging and system integration have been made, the concomitant increase in sensors, actuators, and systems associated with diagnostics, controls, or safety, has resulted in an increase in the number of troublesome electrical contacts. Because current and voltage specifications alone do not provide sufficient information to fully describe the system, switches are generally selected on a trial-and-error basis amongst traditional and unoptimized structures which have changed little over the past 25 years.

Impact is a prominent phenomenon in many electro-mechanical systems. Thus in order to correctly simulate and design these systems, impact must be modelled correctly. The solution depends significantly on the hypothesis that is adopted regarding the nature of the collision.

Through a simple example problem that considers a two-link pendulum striking a flat surface, Kane and Levinson [1] pointed out that the classical solution of rigid body impact problems using Newtonian mechanics produces energetically inconsistent results. As evidenced by the recent publications, Kane and Levinson's remarks sparked a remarkable interest in a problem that was thought to have been solved a long time ago. Keller [2] attributed this paradoxical behavior to slip reversals during collision subject to frictional effects. The Newtonian approach ignores the changes in the direction of slip, leading to the overestimation of the rebound velocity as a result of impact [2, 3]. Keller introduced a revised formulation of rigid body collision equations based on Poisson's hypothesis that impact never increases energy. Yet, Stronge [4] has exposed energy inconsistencies in solutions using Poisson's hypothesis when the coefficient of restitution, e, is assumed not to depend on the coefficient of friction. He divided the energy that is dissipated during collision into two portions: dissipation due to frictional impulse and dissipation due to normal impulse. Then, he demonstrated that Poisson's hypothesis does not lead to vanishing dissipation due to normal impulse when the coefficient of restitution is unity (perfectly elastic impact). Stronge proposed an "energetic" definition for e. This definition equates the square of the coefficient of restitution to the ratio of elastic strain energy released at the contact point during restitution to the energy absorbed by deformation during compression.

Shabana and Gau [5, 6] examined the effect of the topological change in the propagation of longitudinal elastic waves in mechanical systems. The application of the analysis presented is demonstrated using a rotating rod that is subject to an axial impact by a rigid mass moving with a constant velocity. On the experimental front, Yigit *et al*. [7] verified the validity of using the algebraic generalized impulse momentum equations of a radially

0022–460X/97/350712 + 09 $25.00/0/sv971040

rotating beam, transversally impacting an external surface. Their conclusion was that the momentum balance method and an empirical coefficient of restitution can be used with confidence in the impact of a radially rotating beam. A spring–dashpot model for the dynamics of a radially rotating beam with impact is studied by the same authors [8].

The impact that appeared to be single to the naked eye consists in reality of several collisions in rapid sequence. Existence of multiple collisions was recognized by Mason [9], Goldsmith [10], and Yigit *et al*. [7, 8].

Stoianovici and Hurmuzula [11] used a discrete model for the dynamics of a flexible bar during the collision process. They sectioned the bar in equal rigid segments, connected to one another by linear springs of uniform stiffness, and placed symmetrically at a specific transverse distance from the neutral axis. The stiffness constant was evaluated by using the axial displacement at the center of a vertically hanged bar caused by its weight. The transverse distance was determined by an equivalence with the rotation of a transversal section, at the center, of a horizontal cantilever bar acted upon by its weight. They consider Lagrange equations for the holonomic case with uniform slip during collision.

In this article the collision, with solid lubrification and in the presence of an electric current, of unconstrained slender bars with a massive external surface has been studied. The friction force was computed using a generalized law. An analytical continuous model has been developed and validated by comparing theoretical outcomes with experimental results.

2. IMPACT EQUATIONS

The system to be analyzed, shown in Figure 1, consists of a slender unconstrained flexible beam B. Consider the collision between B of mass m and a fixed body B' that is bounded by a horizontal plane. When B is undeformed, its co-ordinate system is denoted as $A[\mathbf{b}_1, O, \mathbf{b}_2, \mathbf{b}_3]$. The motion of A in a Newtonian reference frame $N[\mathbf{n}_1, O_1, \mathbf{n}_2, \mathbf{n}_3]$ is prescribed as a function of time. The reference system A rotates and translates with the beam as if the beam were rigid. The problem is to calculate the general motion of the beam (rigid body motion and flexible deformations). Let x be the distance from O (the origin of A) to a generic cross-section of B, when B is underformed.

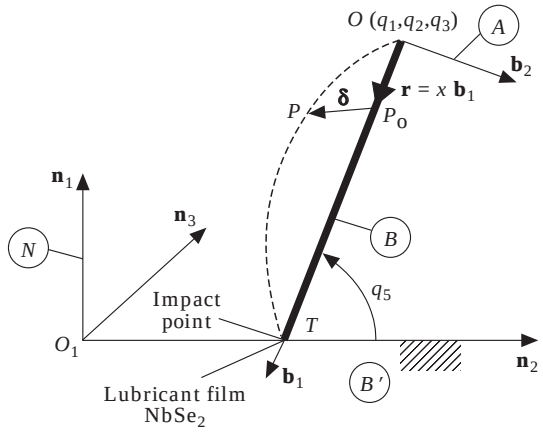

Figure 1. Impact of flexible link with massive surface ($\mathbf{n}_3 = \mathbf{n}_1 \times \mathbf{n}_2$, $\mathbf{b}_3 = \mathbf{b}_1 \times \mathbf{b}_2$).

Inspection of Figure 1 shows that the position vector of an arbitrary point on the deformable beam can be written in N as

$$\mathbf{R} = \mathbf{r}_O + \mathbf{r} + \boldsymbol{\delta}, \tag{1}$$

where $\mathbf{r}_O = q_1(t)\mathbf{n}_1 = q_2(t)\mathbf{n}_2 + q_3(t)\mathbf{n}_3$ is the global position vector of the origin O, and $\mathbf{r} = x\mathbf{b}_1$.

The incident angle vector of the bar at the impact moment is $\{q_4, q_5, q_6\}^{\mathrm{T}}$, where $q_4 = \widehat{\mathbf{b}_1\mathbf{n}_1}$, $q_5 = \widehat{\mathbf{b}_1\mathbf{n}_2}$ and $q_6 = \widehat{\mathbf{b}_1\mathbf{n}_3}$.

The total elastic motion of a generic point $P \in B$ can be expressed as

$$\boldsymbol{\delta}(x, t) = \delta_1\mathbf{b}_1 + \delta_2\mathbf{b}_2 + \delta_3\mathbf{b}_3. \tag{2}$$

Let $s(x, t)$ denote the stretch in the beam along the elastic axis

$$s(x, t) = \sum_{i=1}^{n} \phi_{1i}(x)q_{6+i}(t), \tag{3}$$

where $q_{6+i}(t)$ are the generalized elastic co-ordinates, and $n \in \mathcal{N}$ is the total number of vibrational modes ($\mathcal{N}$ is the set of natural numbers). The transverse elastic displacements are

$$\delta_j(x, t) = \sum_{i=1}^{n} \phi_{ji}(x)q_{3+i}(t), \qquad j = 2, 3. \tag{4}$$

Here, the unrestricted spatial functions $\phi_{ji}(x)$, $j = 1, 2, 3$ are chosen as the mode shapes of a free beam.

The motion of A in N is characterized by the generalized reference speeds

$$u_1 = \dot{q}_i = \mathbf{v}_O \cdot \mathbf{b}_i, \qquad u_{i+3} = \boldsymbol{\omega} \cdot \mathbf{b}_i, \qquad i = 1, 2, 3, \tag{5}$$

where $\mathbf{v}_O$ is the inertial velocity of the point O and $\boldsymbol{\omega}$ is the angular velocity of A in N.

The generalized elastic speeds are defined as

$$u_{6+i} = \dot{q}_{6+i}, \qquad i = 1, 2, \ldots, n. \tag{6}$$

Now, the generalized co-ordinate and speed (reference and elastic) vectors is introduced as

$$\mathbf{q} = \{q_1, q_2, \ldots, q_{n+6}\}^{\mathrm{T}}, \qquad \mathbf{u} = \{u_1, u_2, \ldots, u_{n+6}\}^{\mathrm{T}}.$$

The impact event is initiated when the body B contacts B' at the contact point T. The generalized speeds u_i, $i = 1, 2, \ldots, n + 6$, at the instant t_0 at which B comes into contact with B' are presumed to be known. One seeks to determine the values u_i at the time t_f, the instant at which B completely looses contact with B' (end of collision).

The velocity of an arbitrary point on the deformable beam becomes:

$$\mathbf{v} = \mathbf{v}_O + \boldsymbol{\omega}(\mathbf{r} + \boldsymbol{\delta}) + \dot{\boldsymbol{\delta}}. \tag{7}$$

The velocity of the contact point T is

$$\mathbf{v}_T = v_n\mathbf{n}_1 + v_t\mathbf{n}_2 + v_{t'}\mathbf{n}_3, \tag{8}$$

where v_n is the normal speed, and $\mathbf{v}_t = v_t\mathbf{n}_2 + v_{t'}\mathbf{n}_3$ is the tangential velocity.

The kinetic energy of the beam B is given by

$$K = \frac{\rho}{2}\int_0^L \mathbf{v}\cdot\mathbf{v}\,\mathrm{d}x, \tag{9}$$

where $\rho = m/L$ is the constant mass per unit of length.

The internal forces contribute to the generalized active force, and they can be derived from the strain function of the beam B,

$$U = \frac{1}{2}\int_0^L \left\{E_B\left(\frac{\partial s}{\partial x}\right)^2 + \frac{G_B}{v_B}\left[\left(\frac{\partial \delta_2}{\partial x}\right)^2 + \left(\frac{\partial \delta_3}{\partial x}\right)^2\right]\right\} A_B\,\mathrm{d}x, \tag{10}$$

where A_B is the area of the cross-section, G_B is the shear modulus and v_B is Poisson's ratio (shear area ratio).

The weight mg, where g is the gravity constant, is an external force acting on the flexible link at the center of mass $\mathbf{R}_C$ defined as

$$\mathbf{R}_C = \mathbf{r}_o = L/2\,\mathbf{b}_1 + \boldsymbol{\delta}(L/2, t). \tag{11}$$

In addition the collision between the two bodies leads to contact forces $\mathbf{F}$ at point T, which are written as,

$$\mathbf{F} = F_n\mathbf{n}_1 + F_t\mathbf{n}_2 + F_{t'}\mathbf{n}_3, \tag{12}$$

where F_n is the normal force, and $\mathbf{F}_t = F_t\mathbf{n}_2 + F_{t'}\mathbf{n}_3$ is the tangential force vector.

The normal force exerted by the surface at the contact point can be modelled as a non-linear function of displacement,

$$F_n = ky^{\alpha} + cy^{\alpha}\dot{y}^{\beta}, \tag{13}$$

where y is the normal deflection caused by the impact of the body. Using Hertz theory one has $\alpha = 3/2$. From the literature [8], $\beta = 1$, and this value was assumed to be appropriate for the present study. The stiffness coefficient k at the contact point was estimated from the material properties and the geometry. For the contact between two surfaces, one of them locally plane and the other spherical of radius R, the parameter k is given by

$$k = 0{\cdot}424\sqrt{R}/(h_B + h_{B'}), \tag{14}$$

where h_B and $h_{B'}$ are parameters which are calculated as

$$h_B = (1 - v_B^2)/\pi E_B, \qquad h_{B'} = (1 - v_{B'}^2)/\pi E_{B'}. \tag{15}$$

The damping coefficient, c, of the impact force F_n at the contact point was estimated from an energy balance equation.

The contact force was analytically calculated and examined. The instant when the contact force becomes negative represents the separation of the body and at that moment $F_n = 0$ was set. In this way one can capture the multiple impacts.

When the bar has a non-zero tangential velocity at the onset of the collision $\mathbf{v}_t \neq 0$, there will be a phase of slip. During this phase, the sliding direction can be defined by an angle $\xi = \arctan\,(v_{t'}/v_t)$.

The tangential components of the contract force are

$$F_t = -\mu\cos(\xi)(F_n)^{1-\gamma}, \qquad F_{t'} = -\mu\sin(\xi)(F_n)^{1-\gamma}. \tag{16}$$

where $\gamma = 0$ for dry friction (Coulomb–Morin law of friction). Note that isotropic contact surfaces are assumed which therefore have the same coefficient of friction μ for the two tangential directions.

In this article Lagrange's formalism is used to derive the equations of motion, because it can be easily implemented by using symbolic manipulation programs. For collision, however, an integrated form of equations can be written in matrix form:

$$\mathbf{M}(\mathbf{q})\dot{\mathbf{u}} = \mathbf{C}(\mathbf{q}, \mathbf{u}) + \mathbf{D}(\mathbf{q}, F_n, \mu) \tag{17}$$

where $\mathbf{M}(\mathbf{q})$ is the $(n + 6) \times (n + 6)$ mass matrix, $\mathbf{C}(\mathbf{q}, \mathbf{u})$ is a $(1) \times (n + 6)$ vector which is a complex function of $\mathbf{q}$, $\mathbf{u}$ caused by centrifugal force, Coriolos force, and gravity. The vector $\mathbf{D}$ depends on the pre-impact position and inclination angle and on the normal contact force.

During collision, the relative motion of the contracting end that interacts with the respective surface may change from one case to another (e.g., originally the end may slip in a particular direction, it may then stop and/or slip in another direction). Additional equations can be obtained by considering the relative motions of the contacting end with respect to the surface. Accordingly, the equations that correspond to the possible cases of the motion of the contact point are given as follows.

(1) Since contact is maintained and slip occurs, the normal and tangential components of the contact forces can be represented as

$$|\mathbf{F}_t| = \mu(F_n)^{1-\gamma}. \tag{18}$$

(2) Conversely, when the end does not slip one has

$$\mathbf{v}_t = \mathbf{O}, \text{ subject to } |\mathbf{F}_t|/(F_n)^{1-\gamma} \leqslant \mu \tag{19}$$

(3) On the other hand, when there is no interaction at T, the contact force becomes

$$\mathbf{F} = \mathbf{0}. \tag{20}$$

The procedure is centered around the solution of the set of non-linear differential equations given in equation (17). The structure of these equations depends on the conditions at the contacting end. A change in the relative motion of the contacting end requires the modification of the differential equations. Here a procedure has been developed that automatically detects such changes and implements the necessary modifications to the differential equations to produce consistent results. Starting from a set of pre-impact conditions, the problem is solved in incremental stages. A unique set of equations that reflects the conditions which have to be satisfied at the contacting ends is used at each stage.

The impact equations were solved numerically using a Gears BDF method using IMSL Math/Library [12], and three-mode approximation. Simulations with five and seven modes were also performed, but no detectable differences were observed; thus, a three-mode model was assumed to be appropriate for the current study.

In order to determine the beginning of impact, a numerical algorithm was used [7, 8]. Whenever there is a non-zero contact force, the integration step is backed off and the maximum time step is lowered. This procedure is repeated until a sufficiently small contact force is obtained. The original time step is recovered if there is no sudden change in any of the system variables. This algorithm is essential in order to capture the multiple impacts. For the details about the algorithm the reader is referred to Yigit *et al*. [7, 8].

3. ENERGY BALANCE

The kinetic energy of the system at the instant t_0 at which B comes into contact with B' is the kinetic energy of the *rigid-bar*, K_r. The kinetic energy, $K^+(t_f) = K(\mathbf{q}(t_f), \mathbf{u}(t_f))$, at the instant t_f at which B completely loses contact with B' (end of collision) is computed using equation (9). The work of the normal contact force is computed with the relation

$$L_n = \int_y F_n \, \mathrm{d}y = \int_{t_0}^{t_f} F_n \dot{y} \, \mathrm{d}t, \tag{21}$$

and the energy dissipated by the surface friction is

$$L_t = \int_z F_t \, \mathrm{d}z + \int_w F_t \, \mathrm{d}w = \int_{t_0}^{t_f} F_t \dot{z} \, \mathrm{d}t + \int_{t_0}^{t_f} F_t \dot{w} \, \mathrm{d}t, \tag{22}$$

where z and w are the tangential deflections caused by the impact of the body.

Using the conservation of energy one can write

$$K^-(t_0) = K^+(t_f) + L_n + L_t + U_p, \tag{23}$$

where U_p is the change in potential energy [13].

The damping coefficient, c, of the impact force F_n at the contact point was estimated from equation (23).

4. RESULTS

4.1. *Friction and contact resistance measurements*

A pin-on-disk electro-tribometer was employed for the evaluation of the electrical/tribological properties of the $NbSe_2$ (solid lubricant) film. The electro-tribometer consists of a pin-on-disk assembly, a stepping motor drive system and a constant current/voltage power supply. A personal computer was used to control the experiment and to collect the data. The specimens were moved at a speed of 0·5 mm/s against the tribo pin by computer-controlled stepping motors. Loads from 3–8 N were applied to the tribo arm during the experiments. The friction force and the normal load were recorded continuously by the computer. Constant currents from 0–5 A were provided by a DC power supply. The power supply was also controlled by computer and could by programmed to provide constant current, constant voltage, or current–voltage pulses.

Figure 2 shows the friction force and sliding contact resistance at various loads and currents for burnished $NbSe_2$ film. Tests were performed on virgin films for one pass only to exclude the effects of stick–slip. Each data point represents the average of data measured during sliding.

The friction force increased with increases in load and/or current, as also shown in Figure 2(a). The contact resistance decreased with increases in load and/or current (Figure 2(b)).

For solid interfaces, the generalized law of friction is $|\mathbf{F}_t| = \mu(F_n)^{1-\gamma}$. For the $NbSe_2$ film tested in this study, the exponent γ was 0·7. The coefficient of friction was found to be a function of electrical current (Figure 3), and μ increased with increases in current.

4.2. *Rebound velocity*

The impact was created by dropping the steel link with the length $L = 0{\cdot}3$ m from a variable vertical distance, on a massive block. The end surfaces of the flexible link were

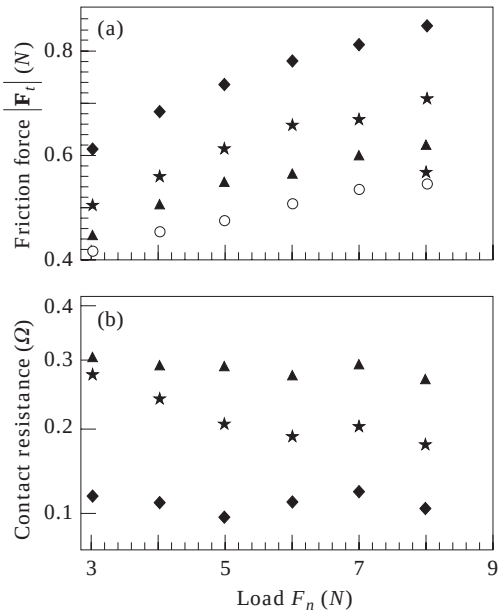

Figure 2. Friction force and contact resistance of burnished $NbSe_2$ films, sliding speed = 0·5 mm/s; (a) friction force, (b) contact resistance. Current levels (A): ○, 0; ▲, 1; ★, 2; ◆, 5.

mechanically polished and subsequently cleaned using both trichloroethane and acetone. $NbSe_2$ films deposited onto the substrate using burnishing. The $NbSe_2$ powders used in the preparation of burnished films were 99·9% pure. $NbSe_2$ was chosen because it has the lowest bulk resistivity among the dichalcogenides. Burnishing was accomplished by manually rubbing the substrate surface against $NbSe_2$ powders for ≈ 30 m.

The pre-collision velocities and orientations of the bar were adjustable. These experimentally measured pre-collision data, were considered as initial conditions for the computer simulated model. A high speed video system was used to acquire the kinematic data. During the collision the elastic deformations of the bar could not be detected on the video images. Therefore, the experimentally obtained kinematic data only reflects the general rigid body motion of the bar. The contact between the bar and the surface was used as a switch in an electrical circuit. Electrical constant currents were provided by a DC power supply controlled by computer.

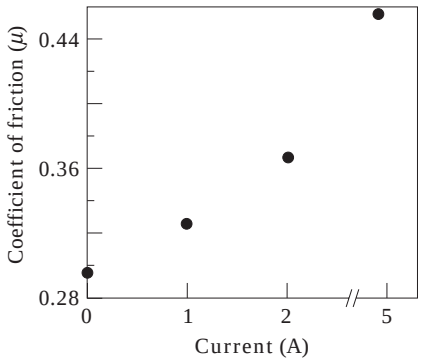

Figure 3. Coefficient of friction.

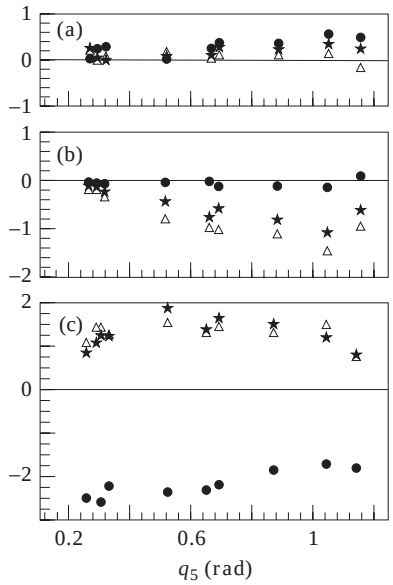

Figure 4. Simulated and experimental kinematic data: (a) tip speed at contact in end $\mathbf{n}_3$ direction; (b) tip speed at contact in end $\mathbf{n}_2$ direction; (c) tip speed at contact in end $\mathbf{n}_1$ direction; ●, experimental and simulated data before impact; △, experimental data after impact; ★, simulated data after impact.

Figure 4 depicts experimental and computer simulated data for the flexible bar using an electrical current of 1A. The simulated results are in good agreement with experimental data. Using the same initial conditions from the free fall of the bar, there is a good fit between simulated and experimental data for the tip velocity of the link.

The experimental and numerical results demonstrated that the kinematic coefficient of restitution (computed as the ratio between post and pre-impact normal velocities at the contact point) varied as a result of changing the incidence angle of the bar (Figure 4(c)). The primary reason in the variation of the normal rebound velocity was the vibrations of the bar. These vibrations are tied to the motion of the tip of the bar with respect to the impact surface during collision. For a wide variety of circumstances, the rigid body assumption does not coincide with the experimental data [11]. The results obtained by rigid body dynamics are dissimilar to experimental data. In reality, the disturbance generated at the impact point propagates into the interior of the bodies with a finite velocity, and its reflection at bounding surfaces produces oscillations or vibrations in the solid.

5. CONCLUSIONS

The analysis method developed in this paper provides a more realistic dynamic model for electrical contacts and switches. The model is complex and provides and effective way of predicting the system response taking into consideration contact lubricants, electric current, and impact dynamics.

ACKNOWLEDGMENTS

The author would like to express his gratitude to Professor Bruce J. Tatarchuk for his helpful suggestions, and to Mr. Harish Waghray for the electro-tribometer measurements.

REFERENCES

1. T. R. KANE and D. A. LEVINSON 1985 *Dynamics: Theory and Applications*. New York: McGraw-Hill.
2. J. B. KELLER 1986 *American Society of Mechanical Engineers Journal of Applied Mechanics* **53**, 1–4. Impact with friction.
3. R. M. BRACH 1989 *American Society of Mechanical Engineers Journal of Applied Mechanics* **56**, 133–138. Rigid body collisions.
4. W. J. STRONGE 1990 *Proceedings of the Royal Society* **431**, 169–181. Rigid body collisions with friction.
5. W. H. GAU and A. A. SHABANA 1991 *American Society of Mechanical Engineers Journal of Vibration and Acoustics* **113**, 532–542. Use of the generalized impulse momentum equations in analysis of wave propagation.
6. W. H. GAU and A. A. SHABANA 1992 *American Society of Mechanical Engineers Journal Mechanical Design* **114**, 384–393. Effect of a finite rotation on the propagation of elastic waves in constrained mechanical systems.
7. A. S. YIGIT, A. G. ULSOY and R. A. SCOTT 1990 *American Society of Mechanical Engineers Journal of Vibration and Acoustics* **112**, 71–77. Dynamics of a radially rotating beam with impact. Part 2: Experimental and simulation results.
8. A. S. YIGIT, A. G. ULSOY and R. A. SCOTT 1990 *Journal of Sound and Vibrations* **142**, 515–525. Spring-dashpot models for the dynamics of a radially rotating beam with impact.
9. H. L. MASON 1935 *Transactions of the American Society of Mechanical Engineers* **58**, A55–A61. Impact of beams.
10. W. GOLDSMITH 1960 *Impact*. London: Edward Arnold.
11. D. STOIANOVICI and Y. HURMUZLU 1996 *American Society of Mechanical Engineers Journal of Applied Mechanics* **63**, 307–316. A critical study of the concepts of rigid body collision theory.
12. IMSL MATH LIBRARY 1994 *Subroutines for mathematical Applications*. Houston: Visual Numerics Inc.
13. T. R. KANE, R. R. RYAN and A. K. BANERJEE 1987 *Journal of Guidance, Control, and Dynamics* **10**, 139–151. Dynamics of a cantilever beam attached to a moving base.